0 0 0 0 4 1 0 1 8 7 4

Submitted to Nuclear Physics B

RECEIVED
LAWRENCE
RADIATION LABORATORY

MAY 1 1974

LIBRARY AND
DOCUMENTS SECTION

LBL-2656
Preprint c.1

DOUBLE-CHARGE-EXCHANGE AND INELASTIC SCATTERING IN $\pi^- + {}^3He$

John Sperinde, Don Fredrickson and Victor Perez-Mendez

March 1974

Prepared for the U. S. Atomic Energy Commission
under Contract W-7405-ENG-48

For Reference

Not to be taken from this room

LAWRENCE BERKELEY LABORATORY
UNIVERSITY OF CALIFORNIA
BERKELEY

LBL-2656
c.1

DISCLAIMER

This document was prepared as an account of work sponsored by the United States Government. While this document is believed to contain correct information, neither the United States Government nor any agency thereof, nor the Regents of the University of California, nor any of their employees, makes any warranty, express or implied, or assumes any legal responsibility for the accuracy, completeness, or usefulness of any information, apparatus, product, or process disclosed, or represents that its use would not infringe privately owned rights. Reference herein to any specific commercial product, process, or service by its trade name, trademark, manufacturer, or otherwise, does not necessarily constitute or imply its endorsement, recommendation, or favoring by the United States Government or any agency thereof, or the Regents of the University of California. The views and opinions of authors expressed herein do not necessarily state or reflect those of the United States Government or any agency thereof or the Regents of the University of California.

0 0 0 0 4 1 0 1 8 7 5

DOUBLE-CHARGE-EXCHANGE AND INELASTIC SCATTERING IN $\pi^- + {}^3He$

John Sperinde,* Don Fredrickson and Victor Perez-Mendez†

Lawrence Berkeley Laboratory
University of California
Berkeley, California

ABSTRACT

The reactions $\pi^- + {}^3He \rightarrow \pi^+ + 3n$ and $\pi^- + {}^3He \rightarrow \pi^- + {}^3He^*$ were studied to investigate the T=3/2 three nucleon system. The differential cross sections were measured at scattering angles from 20 to 40 degrees. The secondary pion was momentum analyzed in a magnetostrictive-readout wire-chamber spectrometer. The double-charge-exchange reaction yielded a secondary pion energy distribution, the features of which can be due to either a T=3/2 three-nucleon resonance or a resonance of the nucleons in the ${}^3He$ nucleus. The inelastic scattering reaction yielded a secondary pion energy distribution peaked near threshold, consistent with resonances in both the T=3/2 and T=1/2 three-nucleon systems.

I. INTRODUCTION

The double-charge-exchange (DCX) of π^- on nuclei is a convenient way of producing neutron rich final states. It is particularly useful in the study of the three neutron system since using a target of ${}^3He$ produces the final state of a positive pion and three neutrons. The incident particle, π^-, as well as the final particle, π^+,

---

* Present address: Oximetrix, Mountain View, Calif.
† Also at the University of California, San Francisco.

are both easily detected and their vector momenta can be measured with precision. Since there are only three nucleons in both the initial and final state, the difficulty of separating the three nucleon problem from the four nucleon problem does not arise as it might if the fourth particle were also a nucleon.

The DCX reaction is generally assumed to occur as a cascade of successive charge exchanges on individual nucleons in the nucleus.[1-5] This model correctly accounted for the cross section variations as a function of the total energy and the energy distribution of secondary mesons. However, as pointed out by Becker and Schmit,[6] the calculated angular distributions are peaked in the forward direction, whereas the measured angular distributions are almost isotropic. They interpret this discrepancy as indicative of the double-charge-exchange taking place preferentially on a pair of nucleons, rather than as a cascade process on individual nucleons.

A general feature of the double-charge-exchange reactions which have been studied is the small deviation of the energy of the secondary pion from the energy distribution predicted by the statistical model.[4,5,7,8] Thus significant deviations from the predictions of the statistical model may be interpreted as the result of final state interactions.

The three neutron system is of particular interest because it is the simplest of the three nucleon systems. There are no coulomb forces, the particles are identical, and the isospin state is pure T=3/2. This system has been theoretically studied by a number of authors.[9-12]

Mitra and Bhasin concluded that the ^3P nucleon-nucleon interaction dominates in the three neutron system. Using separable potentials compatible with the two-nucleon data they estimated that it is possible for the three neutron system to be bound. They gave as the most likely quantum numbers (LSJ) = (1 3/2 1/2), with (1 3/2 3/2) somewhat less likely. Note that spin-isospin independence of nuclear forces implies that a T=3/2, S=1/2 trineutron bound state would be reflected in the T=1/2, S=3/2 three nucleon system.[13] An S=1/2 trineutron would be in contradiction to the T=1/2 scattering data. Okamoto and Davies, using variational techniques and the potential of Pease and Fesbach,[14] also concluded (1 3/2 1/2) is the most likely state but concluded that three neutrons are unbound by approximately 10 MeV. Benohr,[15] assuming the two-nucleon potentials of Afnan and Tang[16] or Eikemeier and Hackenbroich,[17] concluded that there is a resonance about 1 MeV above threshold. He gave the quantum numbers (LS)=(1 1/2) for the resonance. This state corresponds to a P-wave neutron moving in the tail of the virtual deuteron.

Searches for bound states of three neutrons have been carried out by several groups of experimenters.[8,18-20] With the possible exception of the experiment by Adjacic, et al., no evidence of a bound state of three neutrons has been seen. Similar searches have been made for the corresponding bound state of three protons with the same negative results.[21,22] At the present time the non-existence of a bound state of three neutrons seems well established. Subsequent work on the T=3/2 three nucleon system has been concentrated on the search for resonances in the continuum spectra of several different reactions.[8,23-26]

In all the reactions studied, distributions which differ from phase space have been obtained. These deviations have been interpreted in various ways by the different groups of experimenters. Tombrello and Slobodrian conclude that the triton spectrum obtained from the reaction $^3He(^3He, t)3p$ at 50 MeV is distorted by the Coulomb interaction of the triton and the three protons. Kaufman, et al., suggest that the proton spectrum obtained from the reaction $^4He(\pi^-,p)3n$ at 140 MeV may indicate a three-neutron resonance. Ohlsen, et al., report that their data from the reaction $^3H(t,^3He)3n$ at 22 MeV suggest the existence of a virtual state in the three neutron system in the range 1.0 to 1.5 MeV above the three-neutron mass. Bacher, et al., explain the departure of their energy spectrum from phase space in the reaction $^3He(p,n)3p$ at 25 MeV as a $^1S_0$ final-state interaction between two protons. Williams, et al., studied the same reaction at 50 MeV and interpreted their results as as indicating a three proton resonance at 16±1 MeV excitation energy relative to the ground state of ^3He. It is apparent from the diversity of the above interpretations that a model is needed which can simultaneously explain the results of the above experiments as well as additional experimental evidence against which such models can also be checked. Of particular interest are experiments which do not have the possible limitations of the above, such as the coulomb interactions in the Tombrello experiment, the π^- capture reaction on a proton-proton pair which could produce results similar to those obtained in the experiment of Kaufman, et al., and the complications introduced by a fourth nucleon in several of the above reactions. Such an experiment is the study of the DCX reaction π^- on ^3He.

II. EXPERIMENTAL METHOD AND APPARATUS

A. General Method

This experiment was designed to observe reactions of the type $\pi^- + {}^3He \rightarrow \pi^\pm + X$, with the invariant mass distribution of X the main quantity of interest. The invariant mass of X can be determined by measuring the vector momentum of the scattered pion for a fixed energy pion beam incident on a target of ^3He. Reactions leading to charged particles in the final state include the following (assuming no pion production):

$$\pi^- + {}^3He \rightarrow \pi^- + {}^3He \qquad \text{-- elastic scattering}$$

$$\left.\begin{array}{l} \pi^- + {}^3He^* \\ \pi^- + p + d \\ \pi^- + 2p + n \end{array}\right] \qquad \text{-- inelastic scattering}$$

$$\left.\begin{array}{l} \pi^0 + (pnn) \\ \quad \hookrightarrow \gamma\gamma \\ \qquad \hookrightarrow e^+e^- \\ \pi^0 + (pnn) \\ \quad \hookrightarrow \gamma e^+e^- \end{array}\right] \qquad \text{-- charge exchange}$$

$$\pi^+ + 3n \qquad \text{--double-charge-exchange}$$

The elastic and inelastic scattering is of interest both to corroborate the results of the DCX reaction and to check the spectrometer solid angle acceptance using, for instance, the known pion-carbon differential scattering cross section.

A diagram of the experimental setup is shown in figure 1. A beam of π^- of energy 140 MeV (momentum 242 MeV/c) was incident on a target

of ^{3}He. The energy of the beam was selected to be near the $\Delta(1236)$ pion-nucleon resonance so that the DCX cross section would be relatively large and below the pion-production energy-threshold in order to minimize the background reactions. The direction of the incoming π^- was determined with two scintillation counter hodoscopes (A and B). The momentum and direction of the outgoing $\pi^\pm$ were measured with a spectrometer consisting of wire spark chambers, two on each side of an analyzing magnet. The central axis of the spectrometer was at an angle of 30 degrees with respect to the central beam line and allowed the detection of events over a range of scattering angles from 15 to 45 degrees. The DCX cross section was expected to be peaked in the forward direction. The final positioning of the spectrometer was a compromise between the small angle desired from cross section considerations and a large enough angle so that the upstream spark chambers in the spectrometer would not be swamped with beam particles. The maximum solid angle acceptance of the spectrometer was approximately 22.5 msr at 170 MeV/c and decreased on the low momentum side to 9 msr at 100 MeV/c and on the high momentum side to 17 msr at 250 MeV/c (see figure 9). A 0.5 inch thick sheet of aluminum following the last spark chamber stopped the heavy charged particles in the momentum range of interest and prevented them from triggering the system.

The triggering logic consisted of a signal from each of the beam hodoscopes (A and B) and an additional beam counter BP, and signals from a counter C in front of the first spark chamber and a set of counters D behind the fourth spark chamber and aluminum absorber. The

change in the sign of the recorded pion from + to - was accomplished by reversing the direction of the magnetic field in the spectrometer analyzing magnet and adjusting currents in the beam focusing magnets.

B. Beam

The 735 MeV internal proton beam of the LBL 184-inch cyclotron produces pions on striking a beryllium target. The internal target was positioned so that negative pions of 140 MeV produced in the forward direction were bent out of the cyclotron by the fringe field. The extracted particles were further momentum analyzed by a bending magnet in the external pion beam. (See figure 1). Pion fluxes of 2×10^5 π^-/sec with an energy of 140 ± 3 MeV and 0.6×10^5 π^-/sec with an energy of 140 ± 1.3 MeV were obtained with appropriate currents in the quadrapole magnets of the external beam. The beam composition as determined by an integral range curve was found to be 60 ± 10% pions and the remainder electrons and muons. A helium bag was used in the external beam to reduce the scattering of the beam particles.

C. Target

The target consisted of a closed ^{3}He flask and gas reservoir system, and a condenser system using liquid helium as the coolant. A metering-valve regulated the flow of liquid helium into the condenser in which a partial vacuum was maintained. The vacuum lowered the temperature of the helium below the boiling point of ^{3}He, cooling and liquifying the ^{3}He, which was collected in the flask. The density of the liquid ^{3}He was determined by using calibrated carbon resistors to

measure the ^{3}He temperature in the flask. The operating temperature was generally 1.7° K, corresponding to a liquid ^{3}He density of 0.08 gm/cm^3.

A cross sectional view of the target assembly in the region surrounding the flask is shown in figure 2. The flask was a cylinder four inches high and four inches in diameter with a stainless steel top and bottom and with sides of .0075 inch mylar. Situated around the flask were two heat shields, one at liquid nitrogen temperature and one at liquid helium temperature, each consisting of .0005 inch aluminum and .00025 inch aluminized mylar. The entire target assembly was maintained in vacuum to prevent heat transfer to the target. The beam entered and the scattered particles left the target via a .0175 inch mylar window.

D. Magnetic Spectrometer

The magnetic spectrometer consisted of a "C" magnet and four wire spark chambers. The area of the pole tips was 25 × 36 inches. This produced an average bend of 90 degrees over the range of pion momenta from 60 to 260 MeV/c. The vertical separation between pole tips was 8 inches. A 2-inch thick iron slab with a gap of 8 inches was placed on both the entrance and exit sides of the magnet to reduce the extent of the fringing field so that the only significant bending of the particle trajectories occurred in the region between chambers 2 and 3 (see figure 3).

Two wire spark chambers were situated on either side of the analyzing magnet. The redundancy provided by the fourth chamber allowed the rejection of pion decays in flight, scattering from magnet pole tips,

and spurious tracks produced by two different particles. The chambers had the following active areas: chamber (1) 8 × 8 in., (2) 18 × 22 in., (3) and (4) 15 × 55 in. All chambers had four wire planes. In chambers (1) and (2) there was a horizontal plane, a vertical plane and two planes at 45° with respect to the vertical. Chambers (3) and (4) had two vertical planes and two planes at 30° with respect to the vertical. In these two chambers the horizontal coordinate determined the particle momentum. Since the vertical position was not important for the momentum determination some accuracy in the vertical direction was sacrificed for simplicity of construction. For details concerning construction and operation of the chambers, see ref. 27.

Behind the fourth spark chamber was a .5 in. thick sheet of aluminum. Protons and pions having a range of .5 in. of aluminum have a momentum of 330 MeV/c and 85 MeV/c respectively. Since the momentum range of interest was from 60 to 260 MeV/c no protons or higher mass particles could have contributed to the data.

E. Counters and Electronics

Scintillation counters were used in the pion beam to monitor the beam and to determine the incident pion direction and in the spectrometer to detect scattered particles passing through the spectrometer. The positions of the scintillation counters are shown in figure 3. There were three sets of counters (A, B, and BP) in the beam. The four individual A counters each had a sensitive area of 1.5 × 6.0 in. They were overlapped in pairs to define six .75 × 6.0 in. regions. The three B counters were overlapped in pairs to define five .25 × 2.0 in. regions.

The active areas of the individual B counters were: B1 and B3 - .5 × 2.0 in. and B2 - .72 × 2.0 in. The same 1.25 × 2.0 in. region was also covered by the counter BP. All the beam counters were made of 1/32 in. plastic scintillator to minimize scattering. The A and B counters determined the direction of the incoming particle to ± 1.5 degrees in the horizontal direction. Particles passing through the spectrometer were detected by the C counter and the D counters. The dimensions of the C counter are 3.0 × 7.0 in. and it was made of 1/32 in. thick plastic scintillator to minimize scattering. The six D counters were made of .25 in. thick plastic scintillator. Two of them were 12 × 18 in. and the other four were 24 × 18 in. They were arranged in two rows of three each to form a sensitive region 18 × 60 in. All scintillators were coupled by Lucite light pipes to photomultiplier tubes of type RCA 8575 for A, B, BP and C and type RCA 6810A for the D counters.

The signals from the four A counters were mixed as were those from the three B counters. The beam was monitored by the triple coincidence $A \cdot B \cdot BP$. The accidental beam rate was measured by forming the triple coincidence with BP out of time by 208 nsec which corresponds to four cyclotron rf cycles. The signals from the three D counters in each row were mixed and then a double coincidence, $(D_1 + D_2 + D_3) \cdot (D_4 + D_5 + D_6)$, was formed to provide the D signal. The requirement for an event trigger was a signal from D, C, and the beam monitor, $(A \cdot B \cdot BP \cdot C \cdot D)$. This coincidence signal set a gate which disabled the logic for 150 msec, triggered the high voltage pulse to the spark chambers, and strobed a set of flip-flops to accept the signals from the individual A and B

counters. Data for each event were stored on magnetic tape.

The stretched-beam spill of the cyclotron consists of a spike of particles 64 times per second followed by an approximately uniform flux for about 10 msec. The spike was gated off since the flux in this part of the beam spill was too high for our electronics to register properly.

F. Running Conditions

The spectrometer could be set to detect π^-, which was used for $\pi^- + {}^3He$ elastic and inelastic scattering, or π^+, which was used for the double-charge-sxchange reaction. Changing from one mode to the other was accomplished by switching the current polarity in the analyzing magnet. In addition, the focusing magnet currents were adjusted to produce an incident beam with the best energy resolution for the elastic and inelastic scattering measurements where the energy resolution was necessary to distinguish elastic scattering from near threshold inelastic scattering. Since the double-charge-exchange reaction has a small cross section, some energy resolution was sacrificed in favor of higher beam rate. Data were taken with the flask both full and empty. For the target empty runs, the flask was evacuated and thus no corrections to the data were necessary for gas remaining in the flask.

Data were also taken with targets of carbon and ${}^4He$ for calibration purposes.

III. DATA ANALYSIS

A. General

The data analysis consists of taking the experimentally

measured quantities and from them extracting the missing mass distributions in the reactions $\pi^- + {}^3He \rightarrow \pi^\pm + X$. The mass of the recoiling particle X is given by:

$$M_X^2 = 2m^2 + M^2 + 2M(E_b - E_s) - 2E_bE_s + 2P_bP_s\cos\theta \qquad (1)$$

where m is the pion mass, M is the ${}^3He$ mass, E_b is the energy of the beam particle, E_s is the scattered pion energy, P_b is the beam particle momentum, P_s is the scattered pion momentum, θ is the scattering angle, and M_X is the mass of $\left\{\begin{matrix}pnn\\nnn\end{matrix}\right\}$ system. The speed of light c is everywhere equal to one. The quantities P_b, P_s, and θ were determined with the experimental data. The scattering data which were recorded on magnetic tape included the combination of individual A and B counters present in the event trigger and the digitized spark information from each chamber plane. Provisions were made to record two spark positions for each plane.

A computer program used these data to reconstruct each event. The digitized information was used to compute the spark positions in the chambers. The counter data and the sparks in the first two chambers determined a plane and a line whose intersection was the interaction point in the target and whose angle of intersection was the scattering angle. The spark locations in the first three chambers were used to obtain the particle momentum. The spark position in the fourth chamber allowed the discrimination against pion decays in flight, spurious sparks in the chambers, and scattering in the spectrometer. The scattered particle energy and the beam energy were corrected for energy

loss in the target and the spectrometer, and then used in addition to the scattering angle to calculate the missing mass M_X. In elastic scattering this mass corresponded to the mass of ^{3}He which provided a consistency check of the beam energy.

After weighting each event according to the spectrometer solid angle acceptance and pion decay probability, the events were histogrammed as a function of the missing mass. The positron background to the double-charge-exchange data was estimated by the Monte Carlo technique and the final histograms of the data were obtained by subtracting the positron contribution from the experimental data.

A more complete explanation of these calculations is contained in the succeeding sections.

B. Momentum Determination

The spark chamber data consisted of two numbers for each of the four planes in a chamber. The two numbers indicated either zero, one of two sparks and their relative distance from two known fiducial points. A point on the central plane of each chamber was found for which the sum of the squares of the distances to the excited wires was a minimum. For this calculation all chamber planes were assumed to be at the midplane of the chamber. The solutions in those cases where data existed in all four planes were called "4-wire fits". A small percentage (about 3%) of the time one of the planes would not have any data, in which case 3-wire fits were obtained by the same method.

The information used to calculate the momentum of a particle consisted of three points on the particle trajectory and the known

magnetic field. The first two points, which were outside of the magnetic field, fixed the incoming direction of the particle trajectory. Estimates of the momentum (to ±2 MeV/c) and the position in chamber four (to ±0.3 inches) were made by means of polynomials based on wire orbit data and artificially generated events (see figures 4 and 5). An orbit was then integrated through the spectrometer, and the resulting point of intersection with the third chamber was compared to the actual spark location. If the discrepancy was too great, the momentum estimate was improved and further iterations were made. In practice, the accuracy criterion was satisfied for 85% of the events after two orbits.

C. Event Acceptance

The following is a discussion of the event acceptance criteria and the data processing decision made at each step in the analysis:

1. The A and B counter arrays must each have had a signal from a single counter or from a pair of overlapping counters.

2. Each spark chamber had to have at least one spark. A point (determined by the method described in Section B) was considered an acceptable spark if the perpendicular distance to the "worst wire" was less than 0.25 inches in chambers one and two and less than 0.45 inches in chambers three and four. Only 4-wire or 3-wire fits were allowed. By analyzing a portion of the data accepting 2-wire fits, it was found that rejecting the 2-wire fits decreases the efficiency by approximately 2%. More than one spark was allowed but in practice there was usually just one spark per chamber.

3. The intersection of a line (determined by sparks in the first two chambers) with a plane (which represents the incident particle direction) had to be within the target volume. For this test, the target was assumed to be a cyclinder 2.5 inches high and 4.0 inches diameter. Events having their intersections outside of this volume were produced by scattering from the B counters, from the heat shields, and from the vacuum jacket surrounding the target.

4. There has to be a "track" in the first pair of chambers (1 and 2). For those events which survived all previous cuts, a line was computed in which the four planes of each chamber were no longer assumed to be at the central plane of the chamber. For a line to be considered a good track, the perpendicular distance to the worst wire had to be less than .15 inches. If this criterion was not satisfied, the worst wire was discarded and the line recomputed. The event was rejected if fits with fewer than three wires were obtained in either chamber.

5. Tracks in chambers three and four had to make an angle smaller than 45 degrees with respect to the normal to these chambers, since spark location accuracy deteriorates with large angles. The worst wire again had to be within .15 inches of the track.

6. The spark in chamber 4 had to be within 2 inches of the predicted point. This test discriminates against background events produced by pion decay in flight, scattering in the spectrometer, and spurious sparks in the chambers.

7. The particle trajectory had to miss the magnet pole tips by at least .5 inches.

8. The events had to originate in a target volume which was a cylinder 2 inches high and 3 inches diameter. Since the uncertainty in the scattering position was approximately 0.35 inches, events for which the computed scattering position was within 0.5 inches of the flask walls were rejected.

9. The angle between the computed orbit and the track in chambers 3 and 4 had to be small. The requirements were: $\Delta H \leq .012/\sqrt{P}$ and $\Delta V \leq .012/\sqrt{P} + .02$ where P is the particle momentum in BeV/c and ΔH (ΔV) is the tangent of the horizontal (vertical) projection of the angle between the computed orbit and the track. The factor $\sqrt{P}$ in the denominator of ΔH was determined empirically to fit the width of the resultant angular deviations and reflects the fact that multiple scattering is greater for lower momentum particles. The acceptable vertical deviation was much larger than the acceptable horizontal deviation since both the spark chambers and the magnetic field were designed to give the greatest accuracy in the horizontal direction. Figure 6 shows the distribution of ΔH for particles of momentum .240 BeV/c.

Table I shows the fraction of events rejected by each of the above checks for elastic scattering data and for double-charge-exchange data. In the DCX reaction about 75% of the events did not have sparks in all the chambers. Most of these events were accidental coincidences between the D counters and the rest of the triggering logic. Since the trigger rate was approximately 1 per second and since these events were easily rejected in the data analysis, no attempt was made to decrease the fraction of accidental triggers. About 50% of the events having sparks

in all four chambers originated outside of the target volume in both of the above reactions. Such events were due to scattering in the B counters, and heat shields and vacuum jacket surrounding the flask.

D. Errors and Corrections

1. Energy Loss in the Target and Spectrometer.

The incident pion energy was corrected for dE/dx losses in the target. Similarly, the energy of the scattered pion was corrected for losses in the target and in the spectrometer as far as chamber two.

2. Uncertainty in Energy.

The energy resolution was limited almost entirely by the energy spread of the incident beam particles and the multiple scattering of the deflected particles in the magnetic spectrometer. The energy uncertainty in the spectrometer was estimated by assuming multiple scattering occurs only in the region from chamber two to chamber three. This produces a positional uncertainty at chamber three which, using the known momentum variation as a function of position in chamber three, is converted to a momentum uncertainty. While this treatment is not exact, it is a good approximation for our particular geometry. The energy uncertainty (FWHM) as a function of the quantity (M_x-M_{3n}) is shown in figure 7. Folding in the beam energy spread gives the uncertainty in M_x as a function of the quantity M_x-M_{3n} shown in figure 8.

3. Event Weight.

Each event was given a weight which was a function of its momentum and path length through the spectrometer. The factor $4\pi/\Omega(p)$ corrected for the variation of the solid angle acceptance of the

spectrometer as a function of the momentum p. A graph of $\Omega(p)$ is shown in figure 9. The solid angle acceptance is adjusted about ten percent to convert to the solid angle acceptance in the center of mass. The second factor in the event weight corrected for pion decays in flight in the spectrometer and was of the form $\exp(\frac{mD}{P_s \tau})$ where m is the pion rest mass, D is the path length through the spectrometer, P_s is the particle momentum, and τ is the pion lifetime.

4. Background.

A source of uncertainty in the data was the percentage of pion decays which survived all our cuts on the data and appeared to be good events. This fraction has been estimated by the Monte Carlo method to be about 3%. These events consisted almost entirely of pions which scattered in the target and then decayed between the target and the first spark chamber.

The double-charge-exchange data also contained a background of positrons. As stated earlier, particles triggering our system had a range of greater than .5 inches of aluminum, plus .25 inches of plastic scintillator. This corresponds to the range of a 90-100 MeV/c pion, depending on the angle of incidence. All events with a momentum of less than 97.5 MeV/c were assumed to be positrons produced in the reaction

$$\pi^- + {}^3He \rightarrow \pi^0 + pnn$$
$$\hookrightarrow \gamma e^+ e^-$$

The momentum distribution of positrons produced in the above reaction was computed by the Monte Carlo technique. The normalization was obtained by fitting the calculated momentum distribution to the data in the momentum

range of 60 to 97.5 MeV/c. With this normalization the three neutron energy distribution was computed assuming that the positrons were pions and this distribution was then subtracted from the data.

IV. RESULTS

A. Double-Charge-Exchange

A histogram of the raw data as a function of momentum is shown in figure 10. The computed positron spectrum is also given in the same figure. The total number of measured events is ~10,000 of which ~6,000 are estimated to be DCX events. These data are shown in figure 11 as a function of the three-neutron invariant mass after subtracting the positron contribution, and correcting for spectrometer solid angle acceptance (see figure 9) and pion decay in flight. There is no subtraction for target empty runs since the corresponding number of events is negligibly small. The error bars indicate counting statistics. There is an additional 15% normalization uncertainty arising from the uncertainty in the pion beam flux. Figure 12 shows the same data sub-divided according to scattering angle in the ranges of 20-30 degrees and 30-40 degrees.

The cross section normalization was checked using carbon elastic scattering data. A differential cross section of 90 ± 18 mb/sr was measured for elastic scattering on carbon at 30 degrees. This is in good agreement with previous results of 104 ± 6 mb/sr at 150 MeV[28] and 60 ± 15 mb/sr at 125 MeV.[29]

In the energy region corresponding to a bound state of three neutrons there is a fairly uniform background of approximately .02 ± .007 μb/sr-MeV. Given the 6 MeV experimental energy resolution, an upper limit of

.12 μb/sr is obtained for the production cross section for a bound state of three neutrons in the reaction $\pi^- + {}^3He \rightarrow \pi^+ + 3n$.

B. Elastic and Inelastic Scattering

Figure 13 is a plot of the elastic scattering data as a function of the invariant mass of the pnn system. This data is corrected for spectrometer solid angle acceptance and pion decay in flight. In figure 14 the results are presented after subtracting the target empty data. The solid curve is ${}^4He$ scattering data and is normalized to have the same elastic scattering peak height that the ${}^3He$ data has. The ${}^4He$ elastic scattering peak is extrapolated to zero (the dashed curve) and subtracted from the ${}^3He$ data in an attempt to separate the elastic and inelastic scattering. The results are shown in figure 15.

V. DISCUSSION AND CONCLUSIONS

A general feature of many body final states is the fact that the spectrum of one of the emitted particles is given by the statistical model in the absence of any resonances. The solid curve in figure 11 represents the prediction of the statistical model normalized to the data in the energy range of 50 to 85 MeV for the reaction $\pi^- + {}^3He \rightarrow \pi^+ + 3n$. The dashed curve includes the effects of the ${}^1S_0$ interaction between two of the neutrons in the final state. In neither of these cases was any attempt made to include the dynamics of the DCX reaction. However, as stated in the introduction, previous experimental studies of the DCX reaction have all yielded energy distributions with small deviations from the energy distributions predicted by the statistical model. The dot-dashed curve is the result of a somewhat more sophisticated calculation by Phillips.[30] He makes the assumption that double-

charge-exchange occurs by a two-step process and includes the $^1S_0$ final state interaction. He concludes that the formation of a three-neutron system with low kinetic energy is a consequence of the three-nucleons originally being grouped together within the bound state. Calculations of the double-charge-exchange reaction have in the past been able to explain the energy distribution of the secondary pion but the predicted angular distributions have not agreed with the measured results.[4,6] Consequently a comparison of the theoretical and experimental angular distribution could be a sensitive test of Phillips' model were such distributions available. As can be seen in figure 12 no large angular variations are present within the limited angular range of this experiment.

It is interesting to compare our results with the results of Williams et al., for the reaction ^{3}He (p,n)3p at 50 MeV and Kaufman et al. for the reaction $\pi^- + {}^4He \rightarrow p + 3n$ at 140 MeV. Since the reactions involved different particles and were studied at different energies, the magnitudes of the cross sections differ. Suppose there is T = 3/2 resonance in the three nucleon system and that the energy spectrum is determined by the three nucleon final state interaction. Then one would expect the energy spectrum in the energy region close to the resonance to be of the form

$$c|M|^2 PS$$

where c is a constant determined by the particular reaction, M is the matrix element for the three-nucleon resonance, and PS is the four body phase space factor.[31] Figure 16 shows the results of the three

experiments after dividing by the respective phase space factors. The normalization is adjusted to aid in the comparison. The three-proton distribution is shifted by 2 MeV as a rough correction for the Coulomb effects. There is a striking similarity among the distributions--especially the DCX results and the data of Williams et al.--which can be interpreted as evidence for the existence of an isospin 3/2 three nucleon resonance.

The inelastic scattering spectrum is even more sharply peaked near threshold than the DCX spectrum. This is to be expected if there are resonances in both the T = 3/2 and T = 1/2 states as suggested by Batty et al.[32]

If we take the point of view that there are broad resonances in the three nucleon systems, we might arrive at the level scheme shown in figure 17. Assuming then the validity of the evidence from Williams[26] on both bumps, the evidence of Ohlsen et al.,[24] on ^{3}He*, and our own data, we arrive at the level scheme shown.[33] In this scheme we have a quartet of levels T = 3/2 consisting of 3p, ^{3}He*, ^{3}H, 3n. In addition there are two other excited levels in ^{3}He and ^{3}H (Williams, et al.) which can be identified as members of an Isospin T = 1/2 doublet. The parameters of these levels are seen in figure 18 taken from a paper by Batty, et al.[32]

The quantum numbers for the T = 3/2 levels would be (L = 1, S = 1/2, T = 3/2). A model for this object assumes that two neutrons are closely spaced in a virtual $^1S_0$ core with a rather loose L = 1 neutron moving around it with a diameter $\approx$ 5 fermi.[15]

Further experimental work planned is the measurement of the resultant energy distribution as a function of the angle between the incoming π^- and

and the outgoing π^+ and as a function of the incoming π^- energy. Experiments are also planned in which the direction and energy of one of the neutrons is measured. Such experiments should be able to provide considerable additional insight into the existence of a level scheme as described above and into the three nucleon problem in general.

REFERENCES

1. R. G. Parsons, J. S. Trefil, and S. D. Drell, Phys. Rev. 138, B 847.
2. F. Becker and Z. Maric, Nuovo Cimento 36, 1395 (1965).
3. S. Barshay and G. E. Brown, Phys. Letters 16, 165 (1965).
4. Yu A. Batusov, S. A. Bunyatov, V. M. Sidorov, and V. A. Yarba, Yad. Fix. 6, 998 (1967) [Sov. J. Nucl. Phys. 6, 727 (1968)].
5. P. E. Boynton, T. J. Devlin, J. Solomon, and V. Perez-Mendez, Phys. Rev. 174, 1083 (1968).
6. F. Becker and C. Schmit, Nucl. Phys. B 18, 607 (1970).
7. L. Gilly, M. Jean, R. Meunier, M. Spighel, J. P. Stroot, and P. Duteil, Phys. Letters 19, 335 (1965).
8. L. Kaufman, V. Perez-Mendez, and J. Sperinde, Phys. Rev. 175, 1358 (1968).
9. A. N. Mitra and V. S. Bhasin, Phys. Rev. Letters 16, 523 (1966).
10. K. Okamoto and B. Davies, Phys. Letters 24B, 18 (1967).
11. M. Barbi, Nucl. Phys. A 99, 522 (1967).
12. H. Jacob and V. K. Gupta, Phys. Rev. 174, 1213 (1968).
13. L. M. Delves and A. C. Phillips, Rev. Mod. Phys. 41, 497 (1969).
14. R. L. Pease and H. Feshbach, Phys. Rev. 88, 945 (1952).
15. H. C. Benohr, Nucl. Phys. A 149, 426 (1970).
16. I. R. Afnan and Y. C. Tang, Phys. Rev. 175, 1337 (1968).
17. H. Eikemeier and H. H. Hackenbroich, Z. Physik 195, 412 (1966).
18. V. Adjdacic, M. Cerineo, B. Lalovic, G. Paic, I. Slaus, and P. Tomas, Phys. Rev. Letters 14, 444 (1965).
19. S. T. Thornton, J. K. Bair, C. M. Jones, and H. B. Willard, Phys. Rev. Letters 17, 701 (1966).

20. K. Fujikawa and H. Morinaga, Nucl. Phys. A 115, 1 (1968).

21. J. D. Anderson, C. Wong, J. W. McClure, and B. A. Pohl, Phys. Rev. Letters 15, 66 (1965).

22. J. A. Cookson, Phys. Letters 22, 612 (1966).

23. T. A. Tombrello and R. J. Slobodrian, Nucl. Phys. A 111, 236 (1968).

24. G. G. Ohlsen, R. H. Stokes, and P. G. Yong, Phys. Rev. 176, 1163 (1968).

25. A. D. Bacher, F. G. Resmini, R. J. Slobodrian, R. DeSwiniarski, H. Meiner, and W. M. Tivol, Phys. Letters 29B, 573 (1969).

26. L. E. Williams, C. J. Batty, B. E. Bonner, C. Tschalar, H. C. Benohr, and A. S. Clough, Phys. Rev. Letters 23, 1181 (1969).

27. V. Perez-Mendez, T. J. Devlin, J. Solomon, and T. F. Droege, Nucl. Instr. and Methods 46, 197 (1967).

28. T. A. Fujii, Phys. Rev. 113, 695 (1959).

29. J. O. Kessler and L. M. Lederman, Phys. Rev. 94, 689 (1954).

30. A. C. Phillips, Phys. Letters 33B, 260 (1970).

31. K. M. Watson, Phys. Rev. 88, 1163 (1952).

32. C. J. Batty, B. E. Bonner, C. Tschalar, L. E. Williams, A. S. Clough and H. C. Benohr, International Conference on the Three Body Problem in Nuclear and Particle Physics, 1st, Birmingham, Eng. 1969, edited by J. S. C. McKee and P. M. Rolph (North-Holland, Amsterdam, 1970), p. 127.

33. I. Slaus, International Conference on the Three Body Problem in Nuclear and Particle Physics, 1st, Birmingham, Eng. 1969, edited by J. S. C. McKee and P. M. Rolph (North-Holland, Amsterdam, 1970), p. 337.

Table I. Fraction of events rejected by the event acceptance criteria.

Cutoff	Elastic Reject	Elastic Remain	Double-Charge-Exchange Reject	Double-Charge-Exchange Remain
1) Logic	.049	.951	.114	.886
2) Sparks	.071	.880	.744	.142
3) Target intersect	.485	.395	.106	.036
4) Tracks in	.004	.391	.002	.034
5) Tracks out	.005	.386	.002	.032
6) Y4 deviation	.040	.346	.016	.016
7) Pole tips	.085	.261	.004	.012
8) Target 9) Orbit checks	.089	.170	.005	.007

FIGURE CAPTIONS

1. Experimental set-up; MQ, Q1, and Q2 are doublet quadrupole magnets; M is a bending magnet; A,B,BP,C and D are counters, and CH1-CH4 are spark chambers.

2. Target cross section showing the flask, heat shields, and entrance window. The flask was off center so that the beam monitor counters could be as close as possible to the target.

3. Spectrometer setup. CH_1-CH_4 are spark chambers; S_A-S_D are scintillation counters. The aluminum in front of S_D is used to distinguish pions and protons.

4. A histogram of the absolute value of the difference between the polynomial momentum estimate and the final iterated momentum.

5. A histogram of the difference between the polynomial estimated y_4 position and the actual y_4 position for the double-charge-exchange events.

6. A histogram of the tangent of the horizontal angle between the computed orbit and the track given by chambers three and four. The accepted "good" events are indicated.

7. The energy resolution of the spectrometer. The solid line is the resolution for the most probable bending angle in the spectrometer. The dashed lines are the resolutions for the extreme bending angles which were accepted.

8. The energy uncertainty in the missing mass. Curve B is the result for the momentum focused beam. Curve A is the result for the dispersed beam.

9. Spectrometer solid angle acceptance as a function of momentum.

10. Momentum spectrum of the accepted DCX events. The dots are the experimentally measured data. The crosses are the computed positron data normalized to the experimental data with momenta less than 97.5 MeV/c.

11. Energy spectrum of the DCX reaction after subtracting the positron background. The solid curve is 4-body phase space and the dashed curve is 4-body phase space distorted by a $^1S_0$ interaction between two of the neutrons. Both curves are normalized to the experimental data in the energy range of 50 to 85 MeV. The dot-dashed curve is the result of a calculation by Phillips.

12. The energy spectrum for the DCX reaction divided into two angular bins. The crosses are for scattering angles in the range of 30 to 40 degrees, and the dots are for scattering angles in the range of 20 to 30 degrees.

13. The energy spectrum of the ^{3}He elastic and inelastic scattering data. The dots are the target full data and the crosses are the target empty data. The solid lines connecting the points in the elastic scattering peak are only an aid to the eye. Note the scale change at 10 MeV.

14. The energy spectrum of the ^{3}He elastic and inelastic scattering data after subtraction of the target empty data. The solid curve indicates ^{4}He elastic and inelastic scattering results and is normalized to have the same elastic scattering peak height as the ^{3}He data. The dashed curve is the extrapolation to zero of the ^{4}He elastic scattering peak. Note the scale change at 10 MeV.

15. The energy spectrum of the ^{3}He inelastic scattering data. The pd and pnn thresholds are at 5.5 and 7.7 MeV respectively.

16. The energy spectrum divided by phase space factor. The crosses are the reaction $\pi^- + {}^3He \rightarrow \pi^+ + 3n$, the circles are the reaction $p + {}^3He \rightarrow n + 3p$, and the dots are for the reaction $\pi^- + {}^4He \rightarrow p + 3n$. The normalizations of the spectra are adjusted to facilitate comparison. The curves are hand drawn to guide the eye.

17. Possible energy level scheme.

18. Quantum numbers for energy levels. The notation "This Exp." in the figure refers to the experiment of Batty et al.

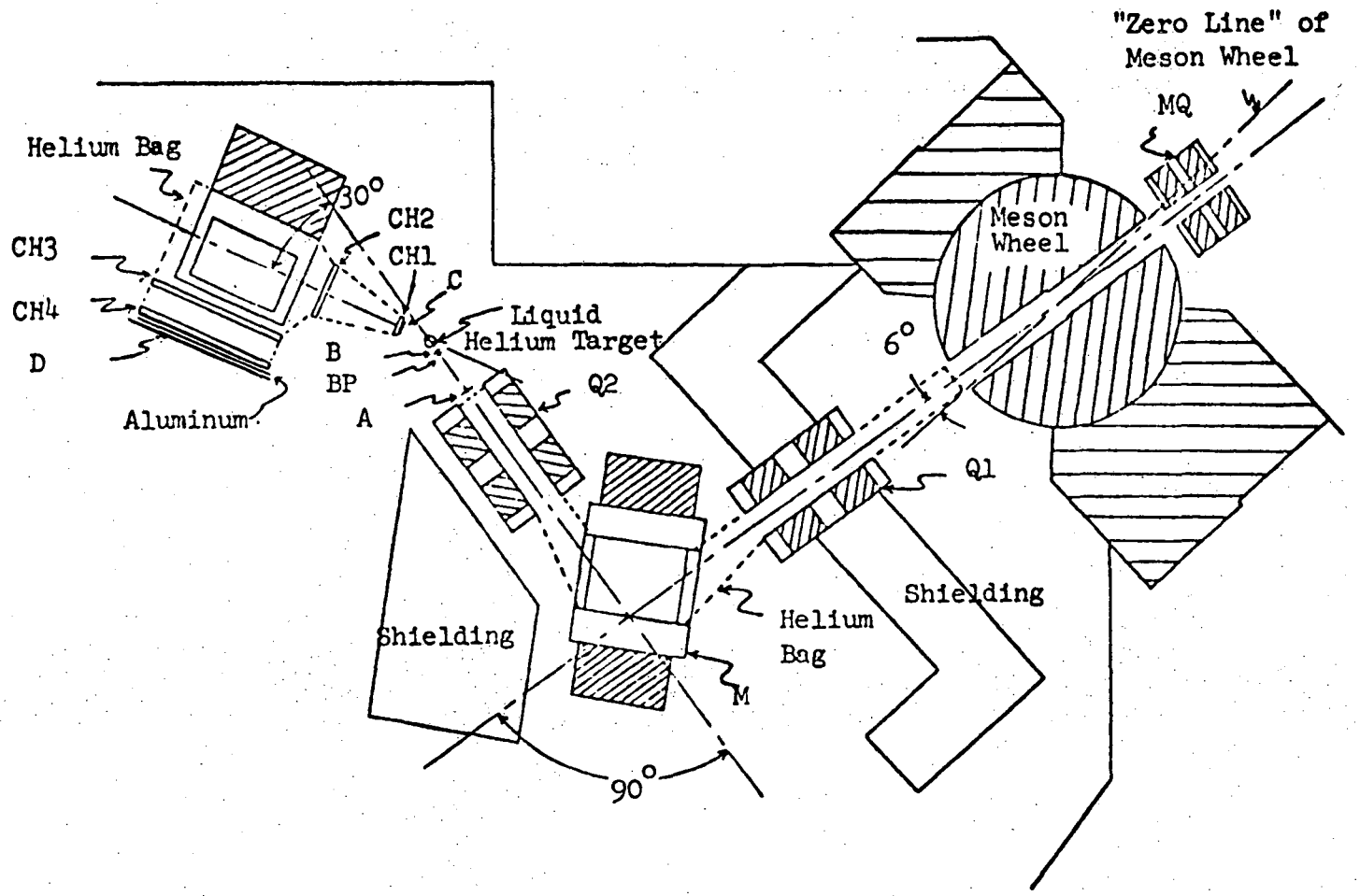

XBL 741-164

Fig. 1.

0 0 0 0 4 1 0 1 8 8 9

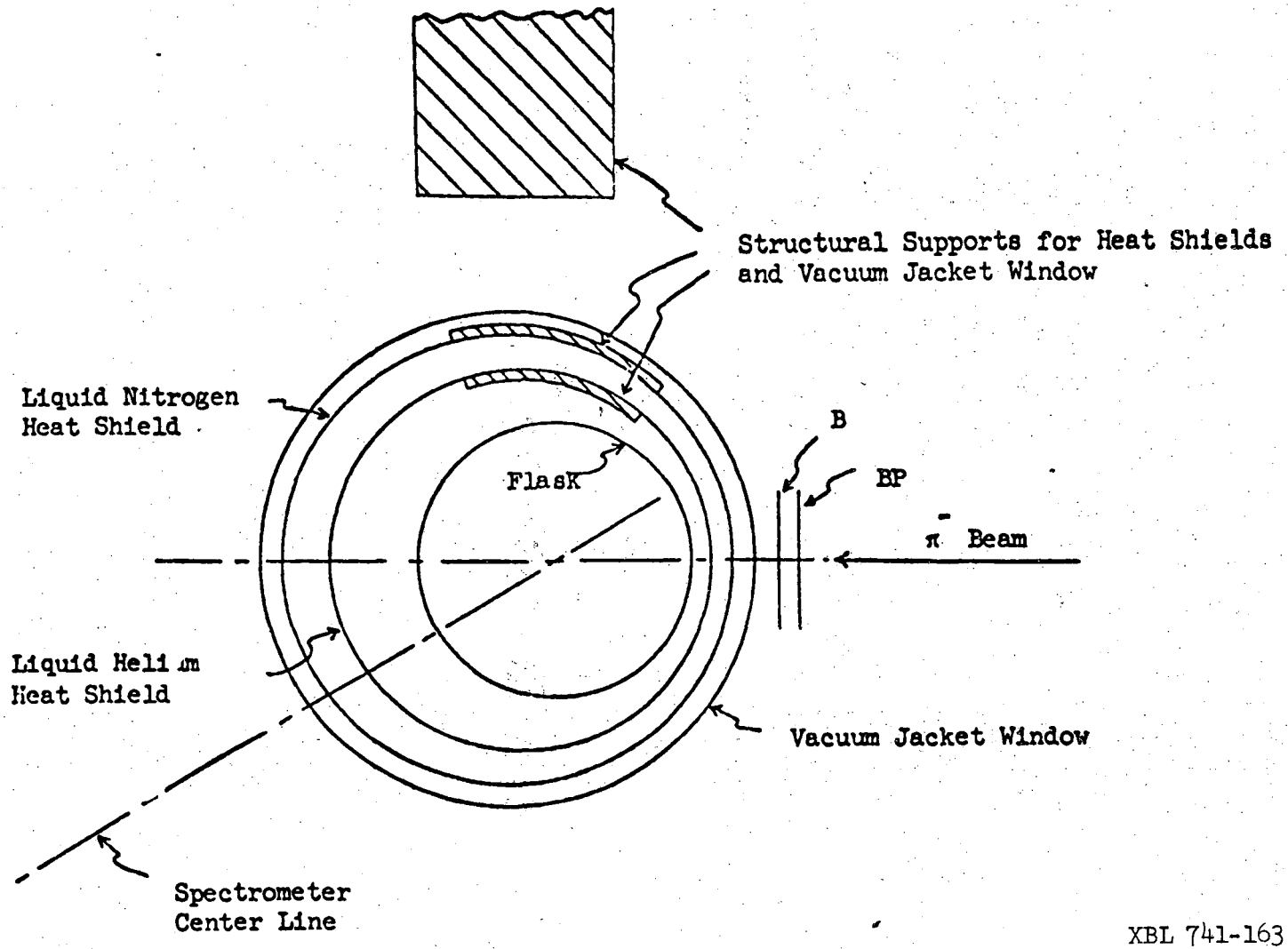

XBL 741-163

Fig. 2.

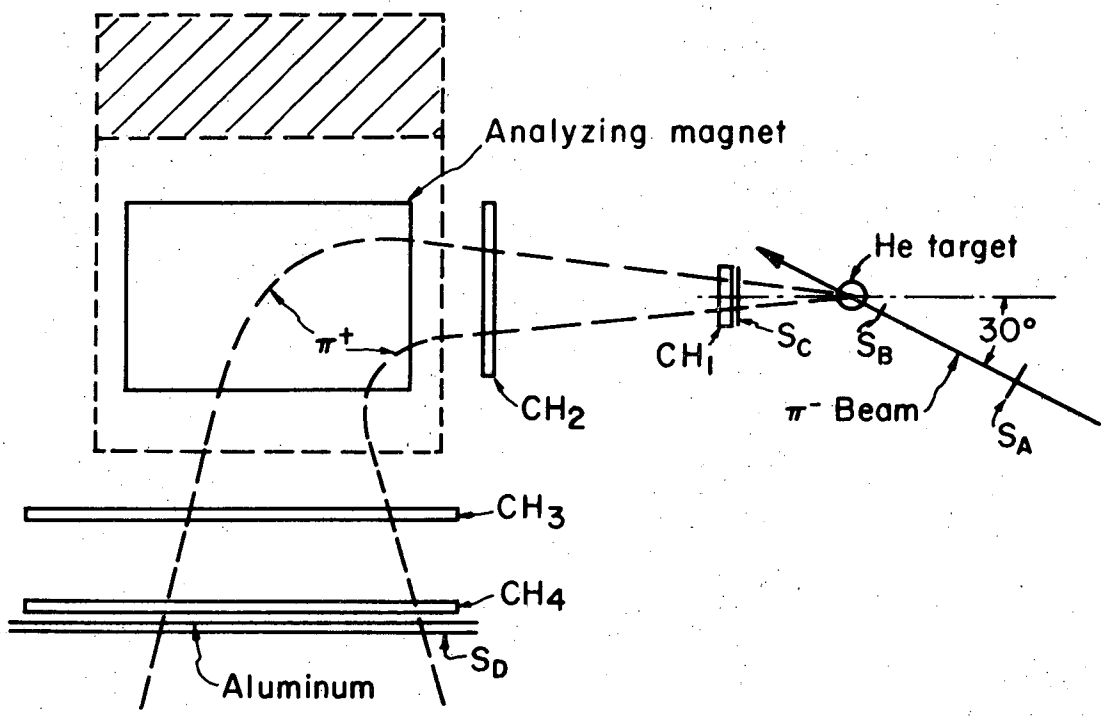

Experimental Setup

XBL704-2680

Fig. 3.

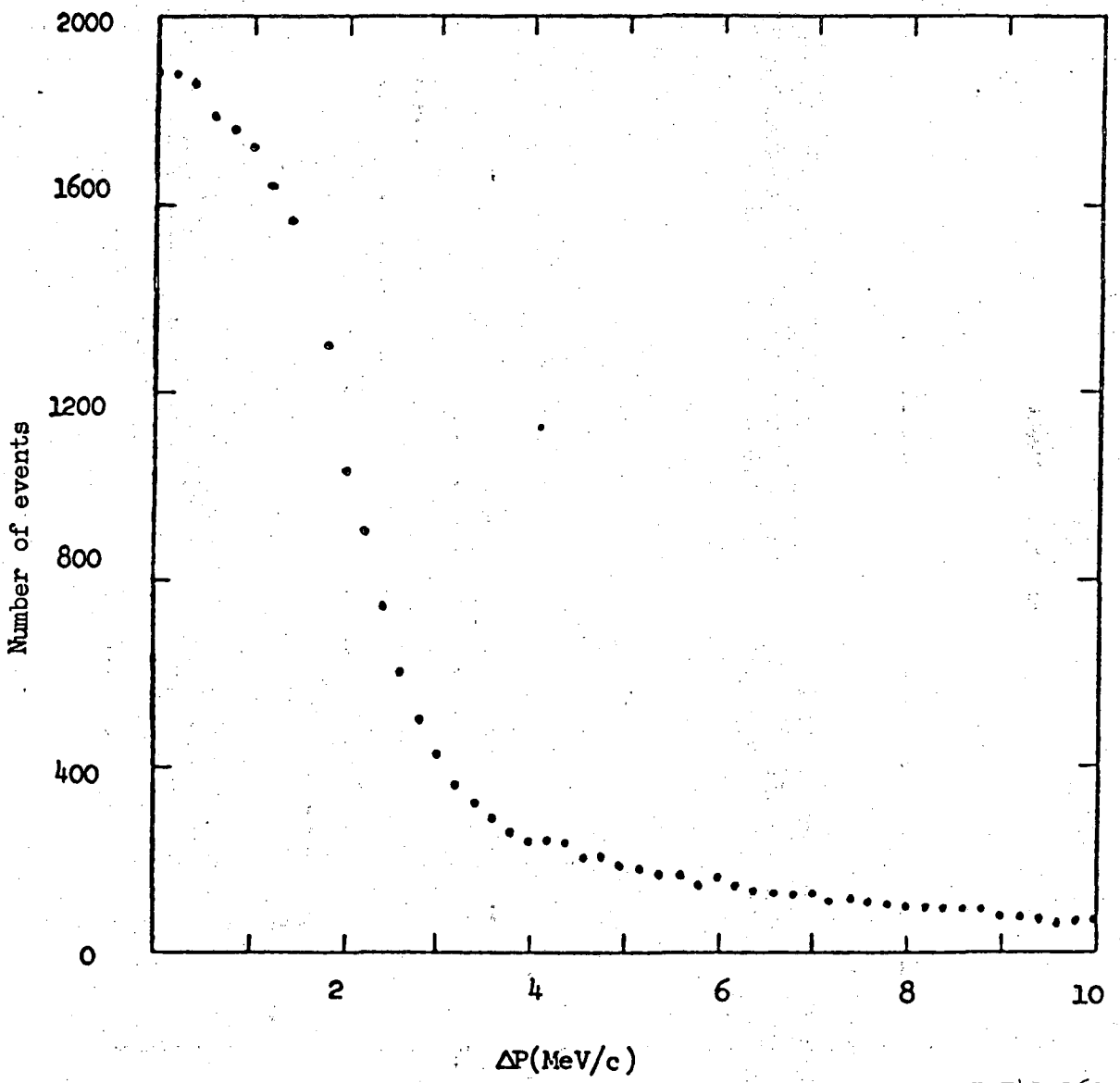

XBL 741-162

Fig. 4.

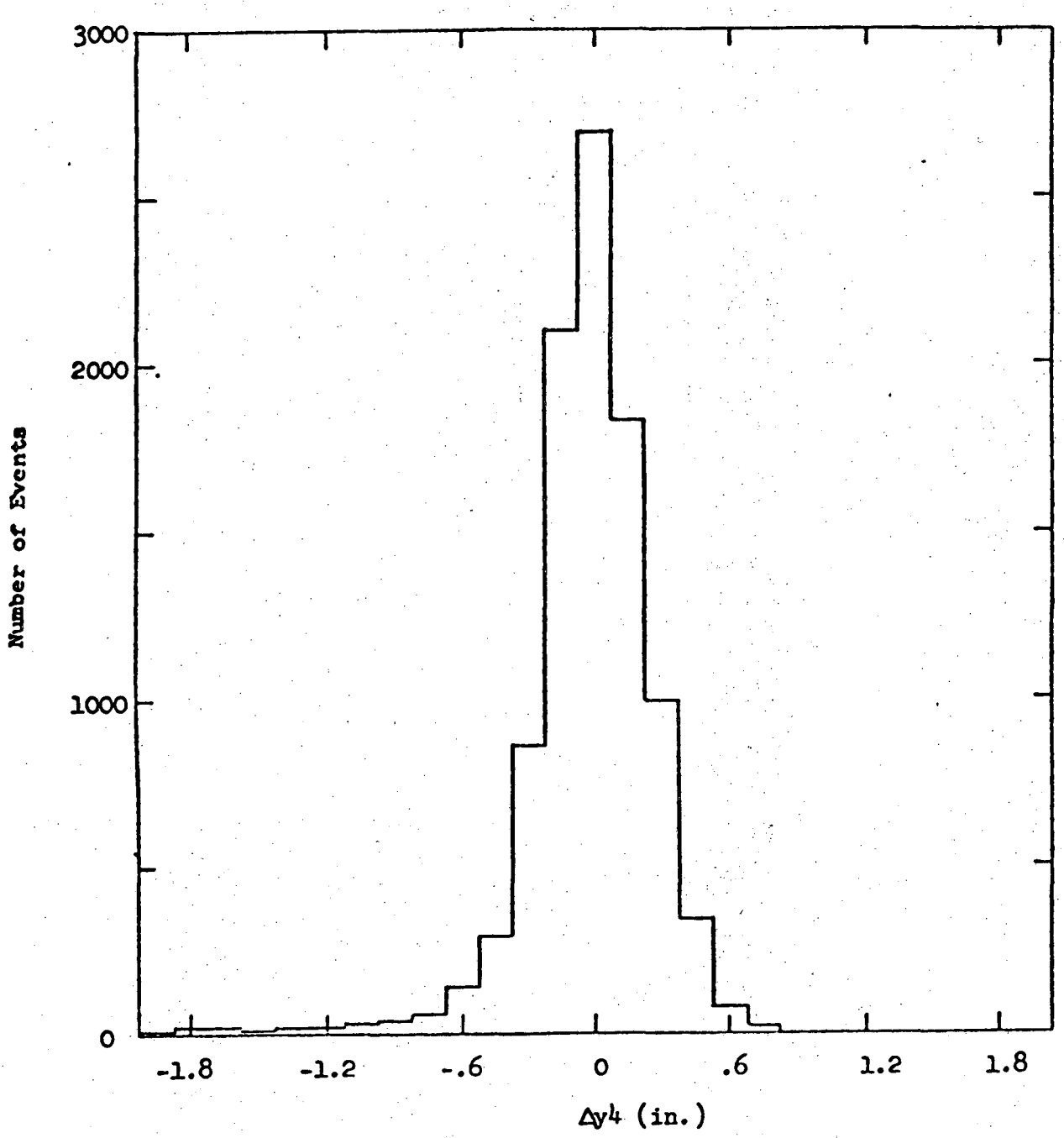

XBL 741-161

Fig. 5.

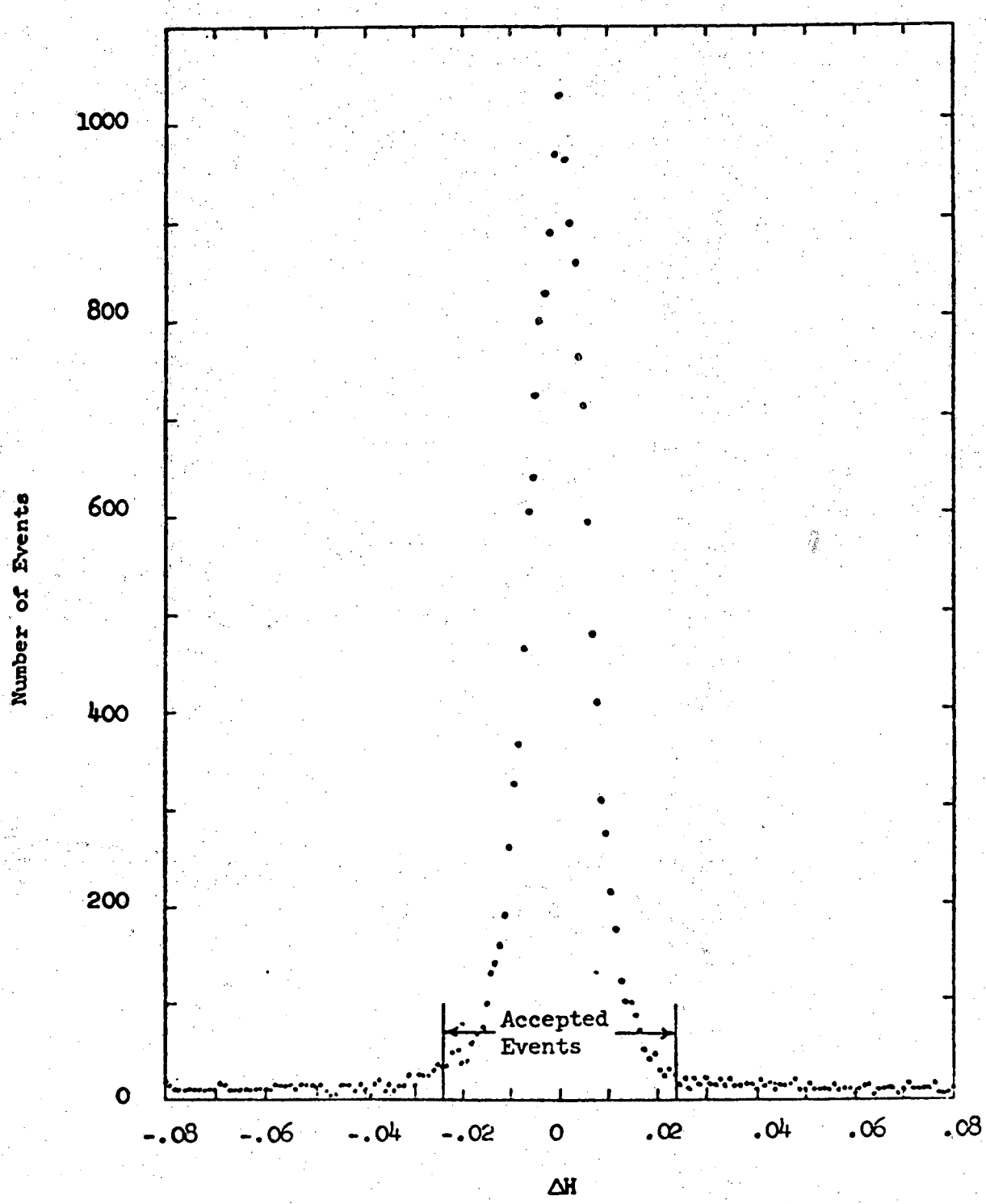

XBL 741-160

Fig. 6.

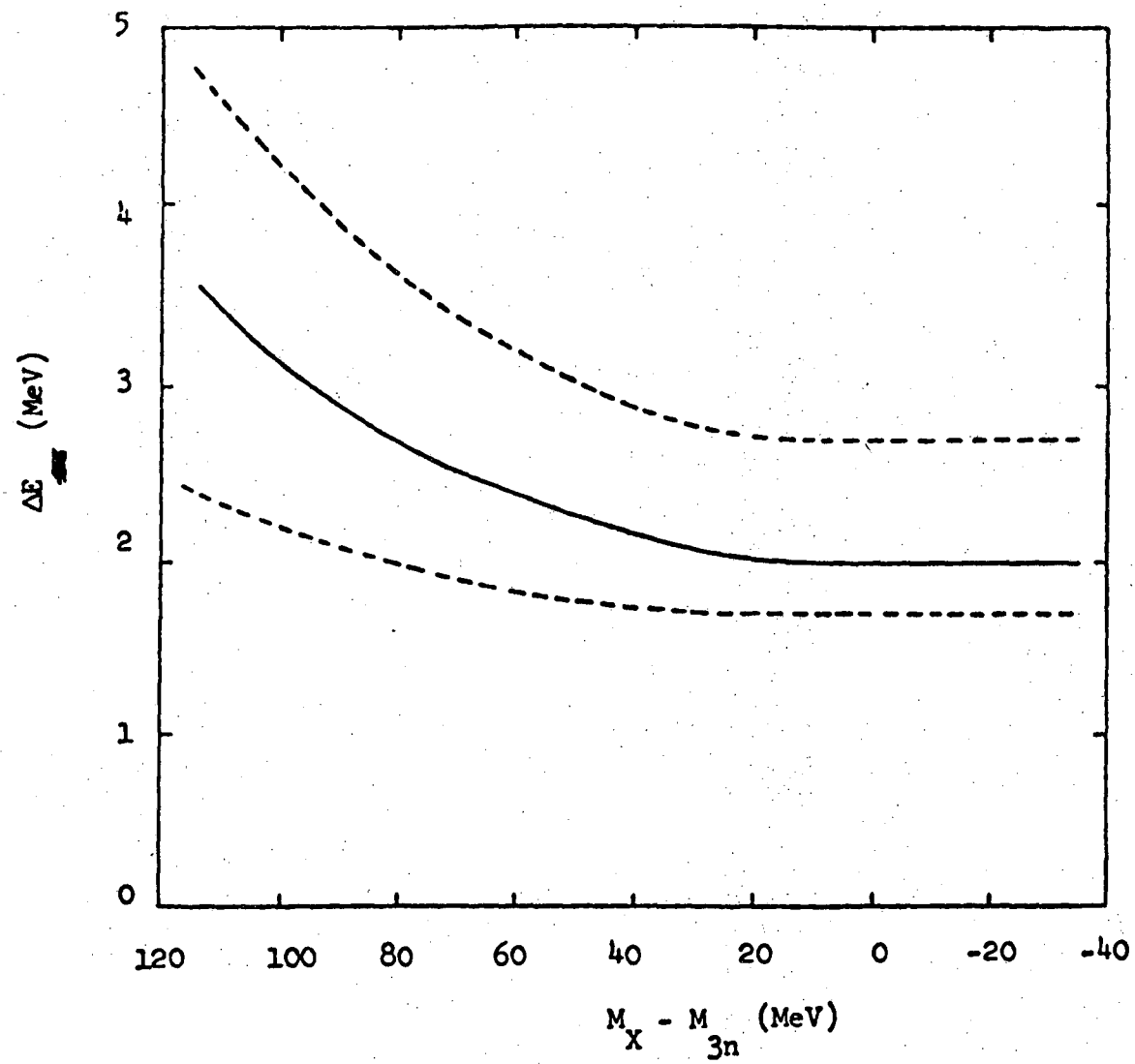

XBL 741-159

Fig. 7.

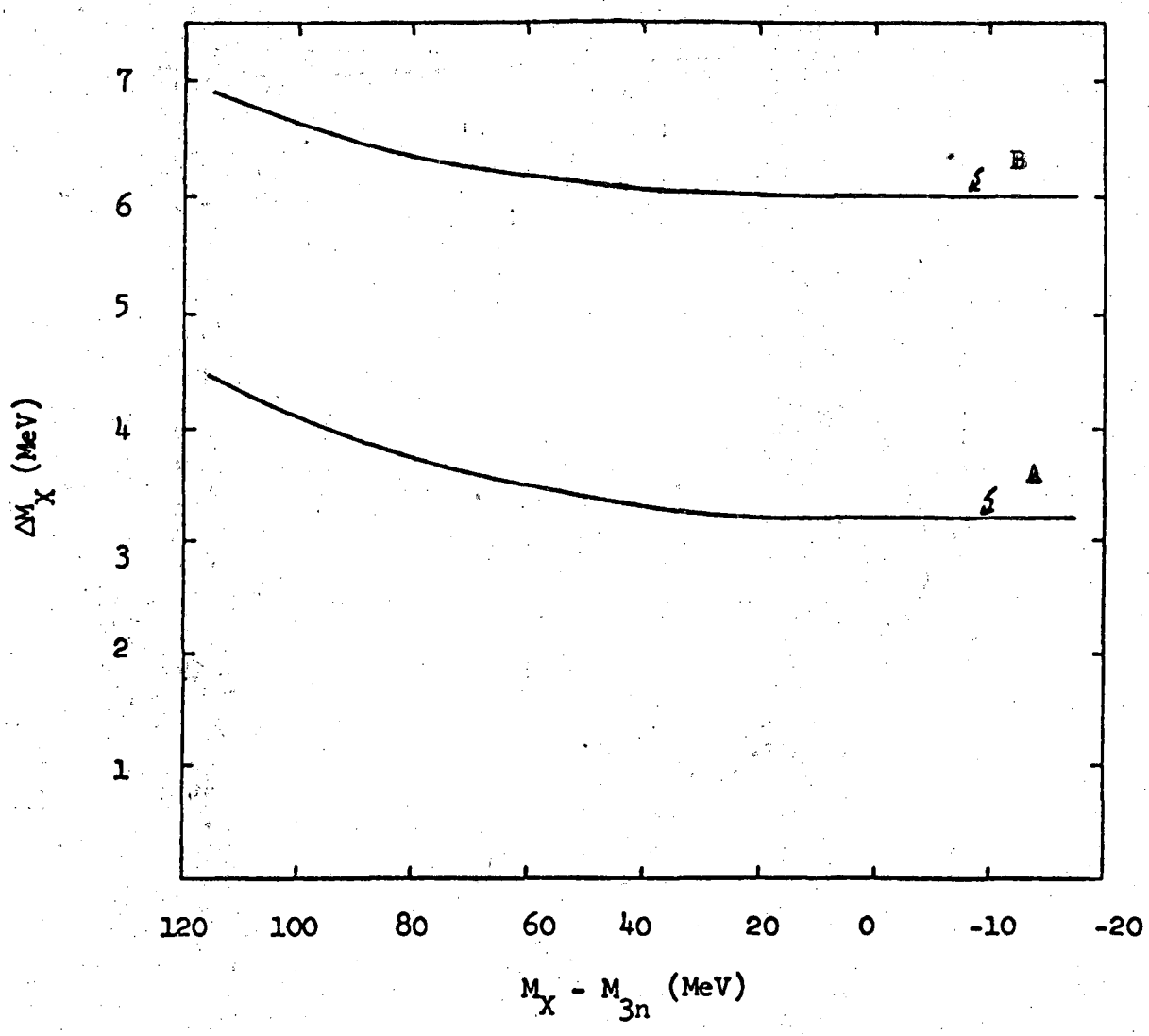

XBL 741-158

Fig. 8.

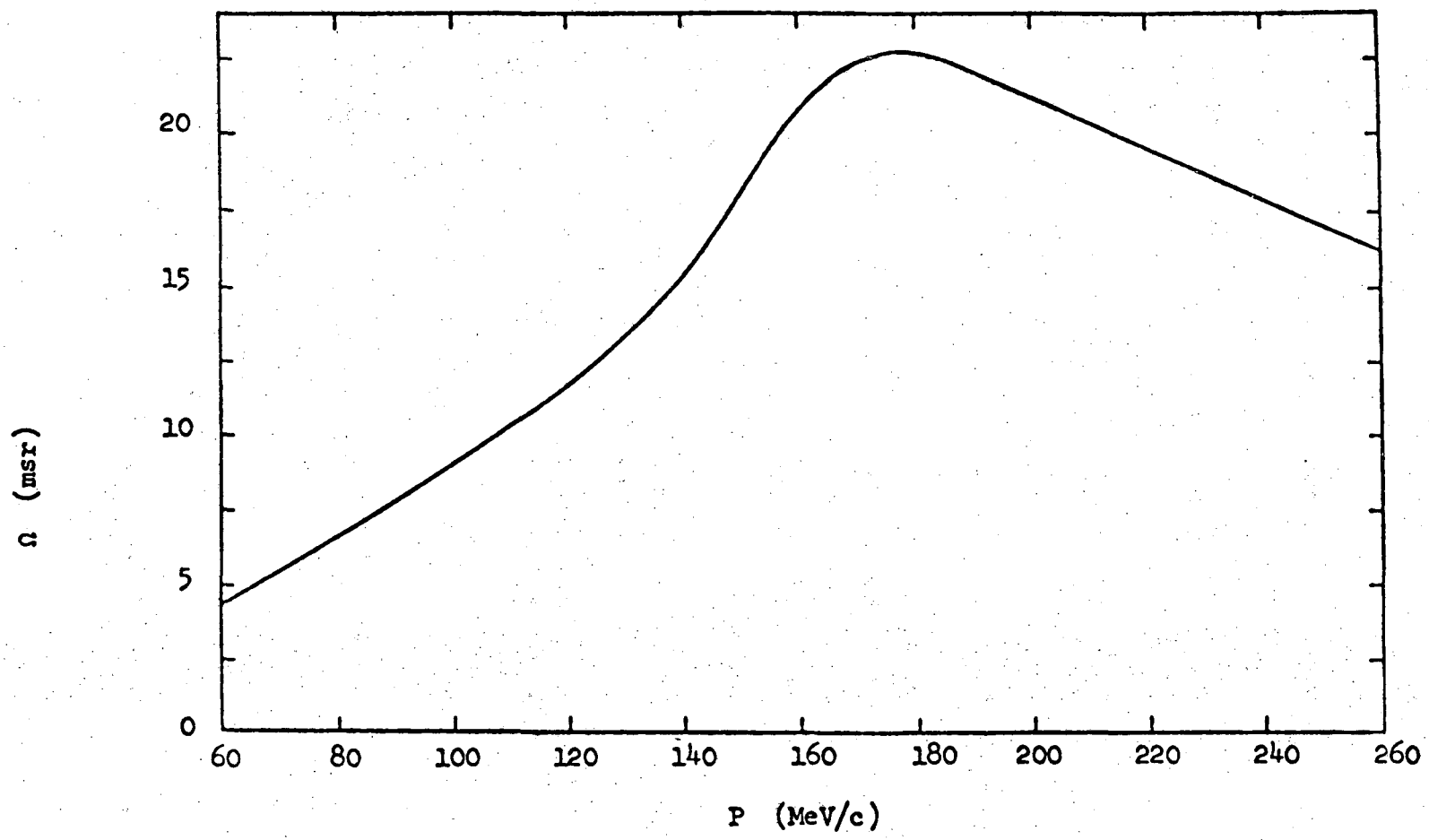

XBL 741-157

Fig. 9.

0 0 0 0 4 1 0 1 8 9 2

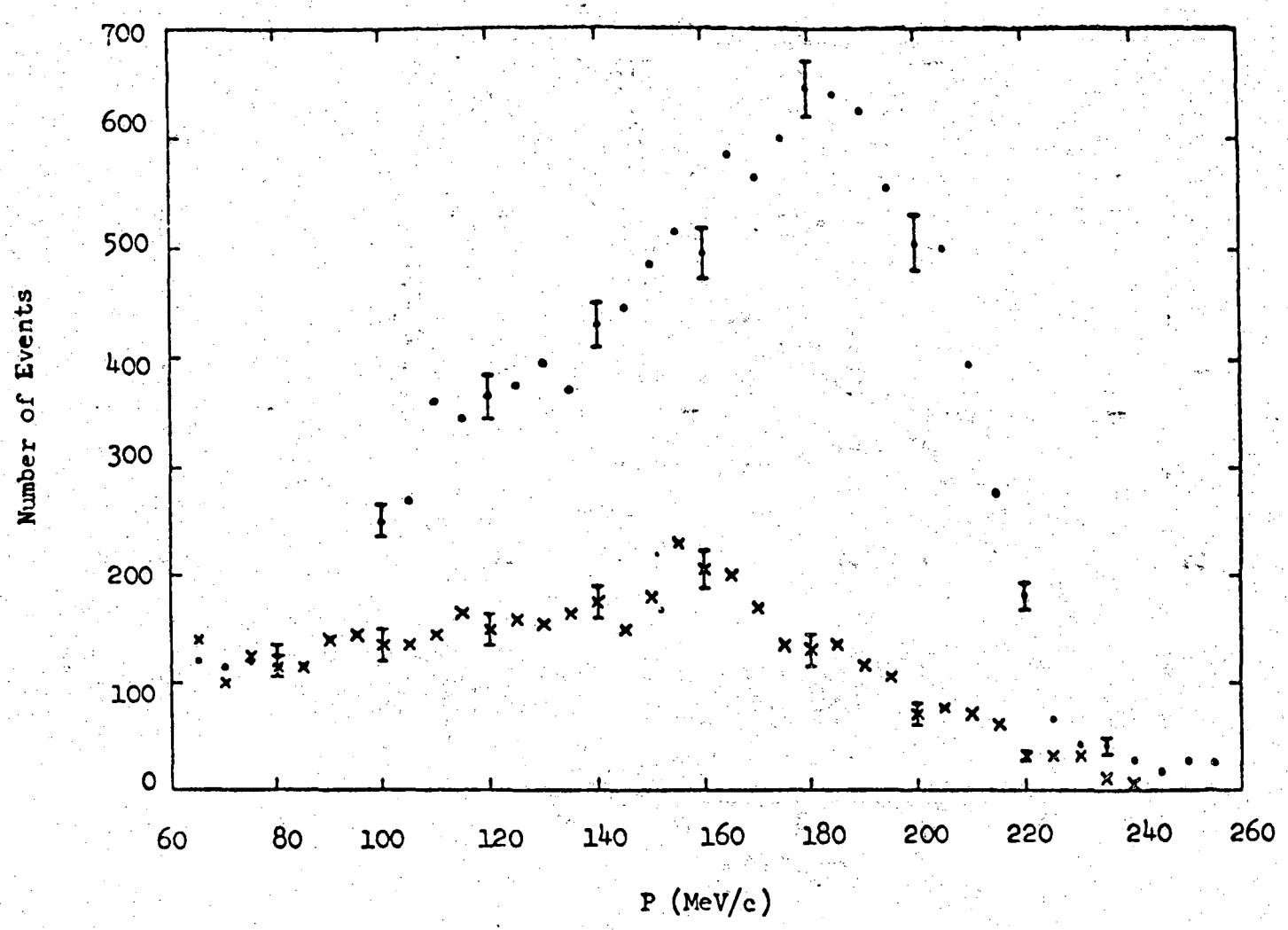

XBL 741-156

Fig. 10.

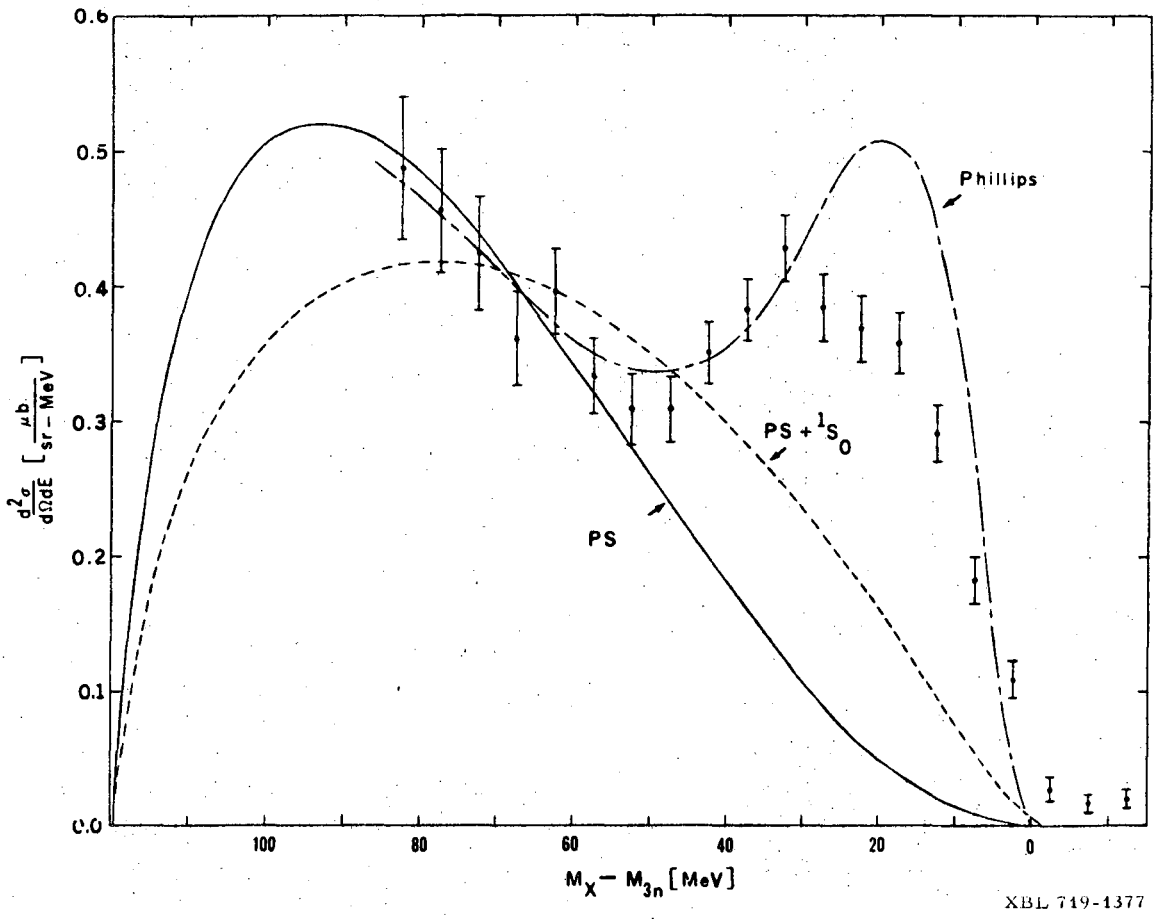
0.6
0.5
0.4
0.3
0.2
0.1
0.0
$\frac{d^2\sigma}{d\Omega dE}$ [$\frac{\mu b}{sr - MeV}$]
100
80
60
40
20
0
$M_X - M_{3n}$ [MeV]
Phillips
PS + $^1S_0$
PS
XBL 719-1377

Fig. 11.

0 0 0 0 4 1 0 1 8 9 3

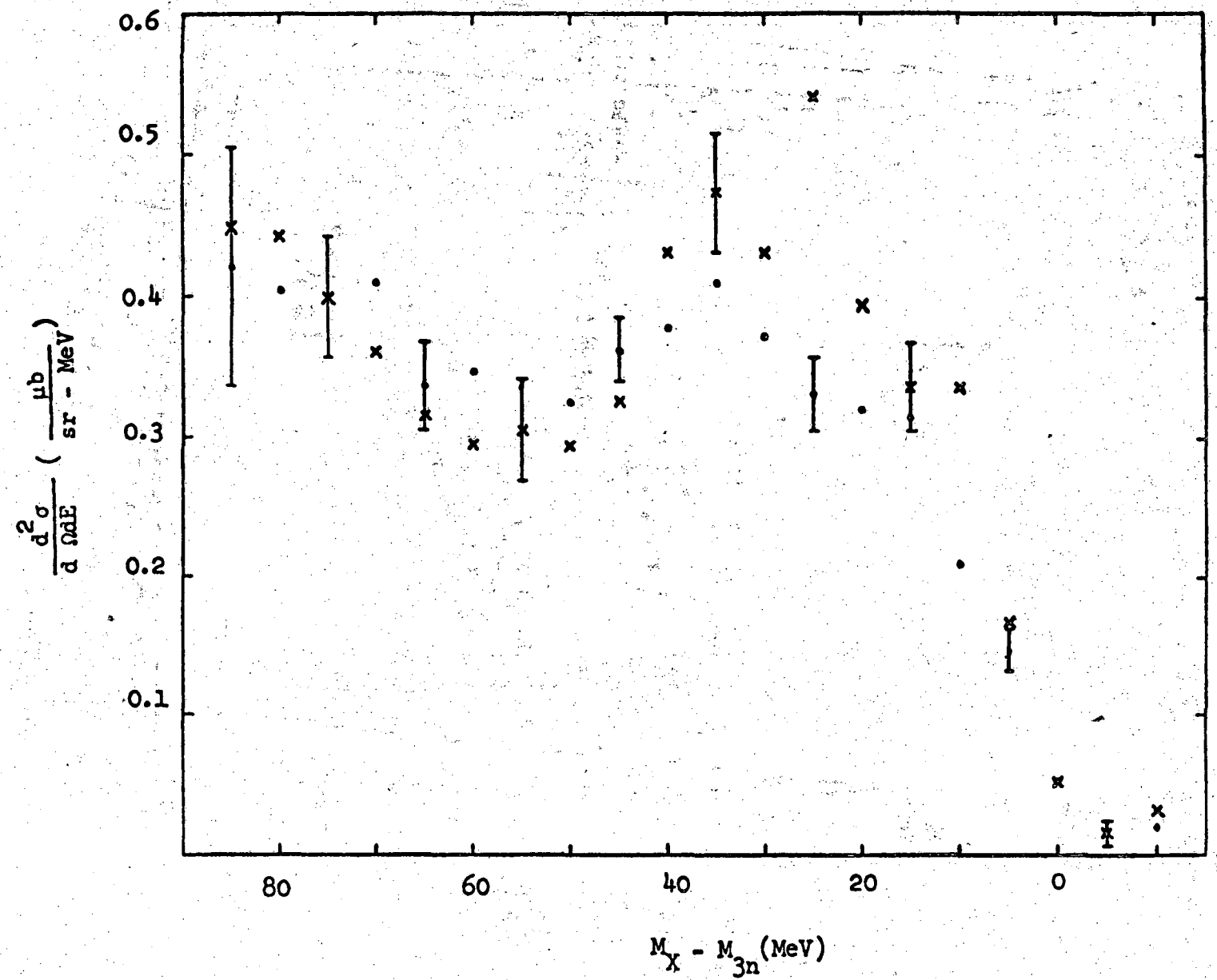

XBL 741-155

Fig. 12.

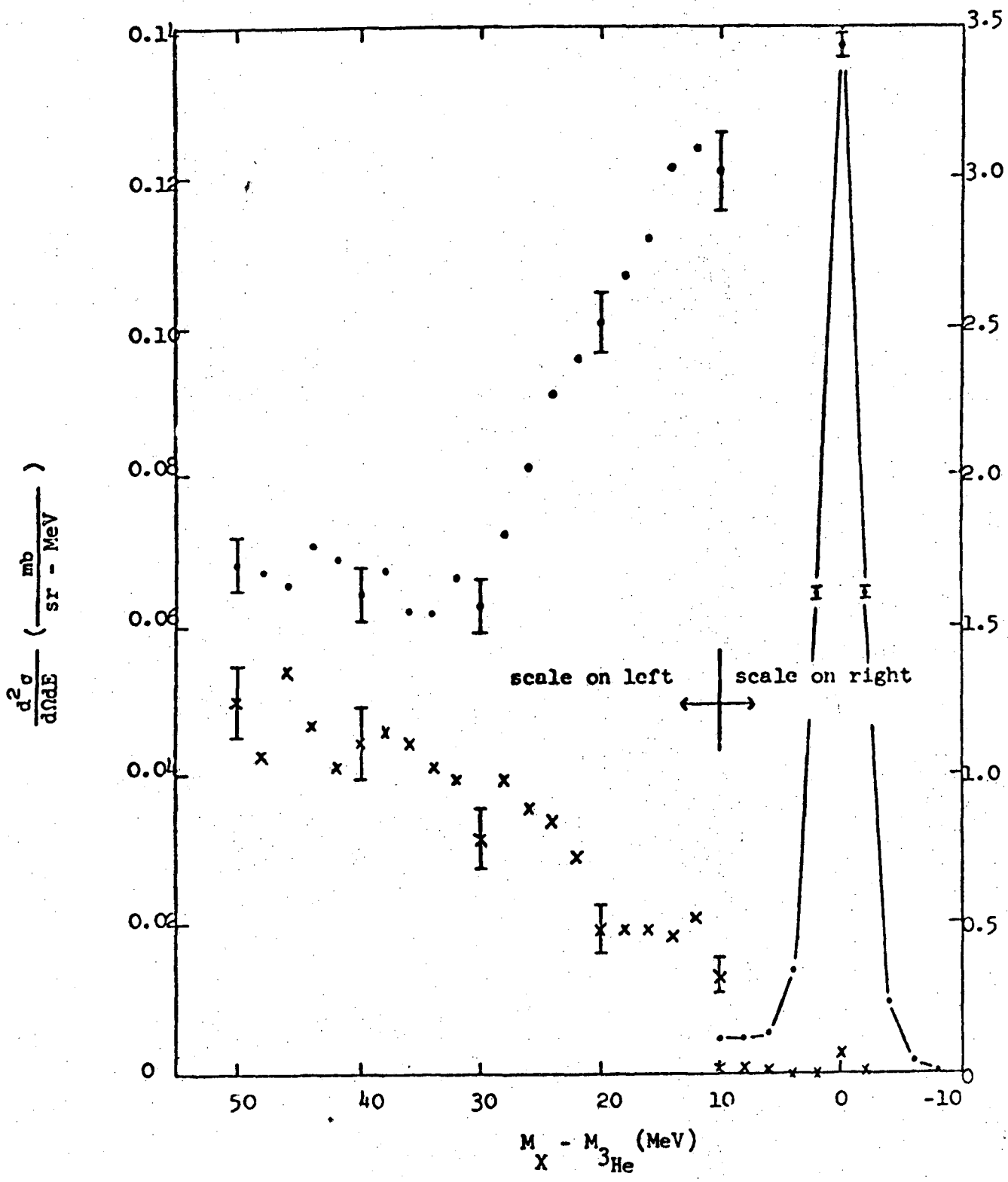

XBL 741-154

Fig. 13.

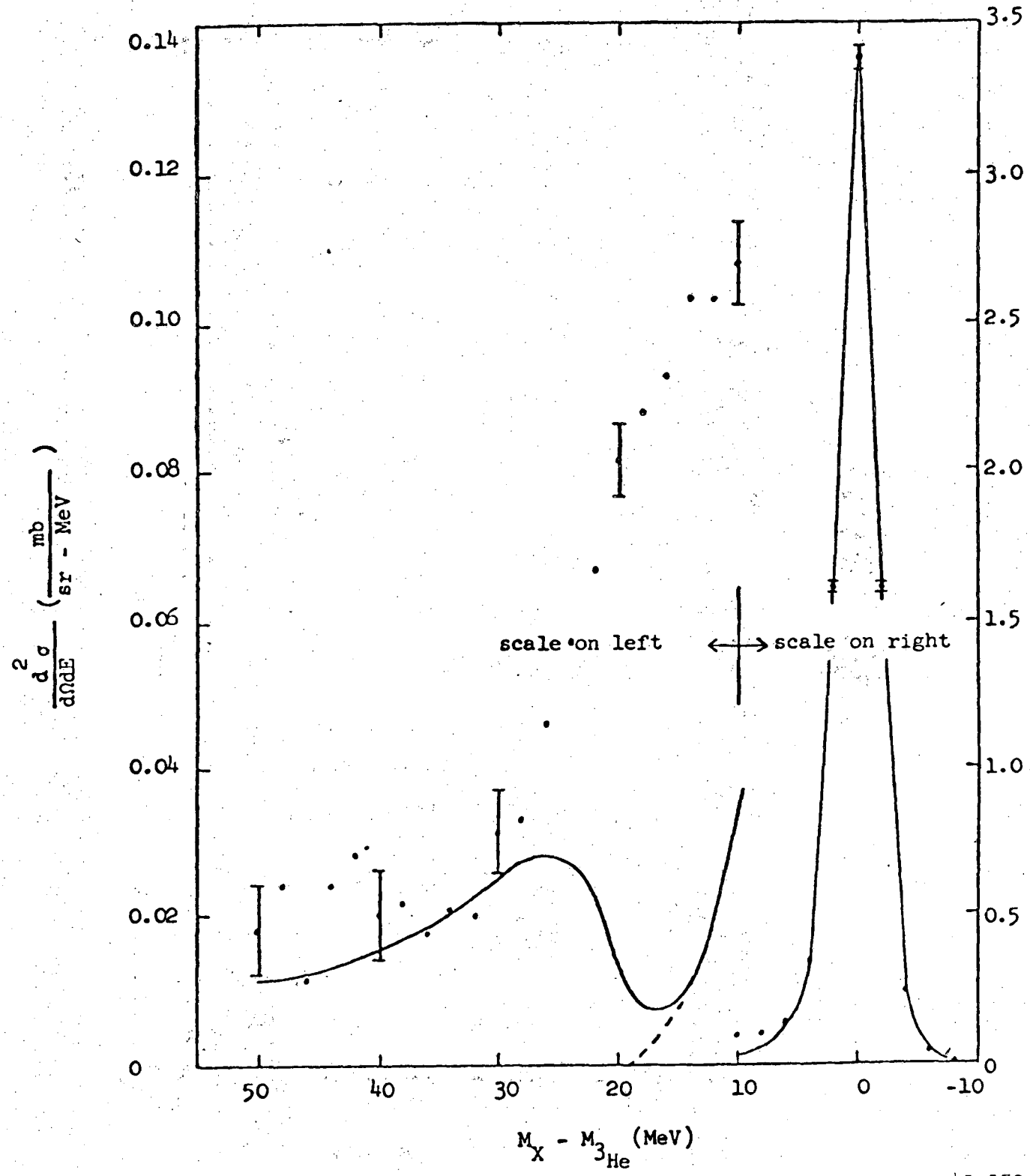

XBL 741-153

Fig. 14.

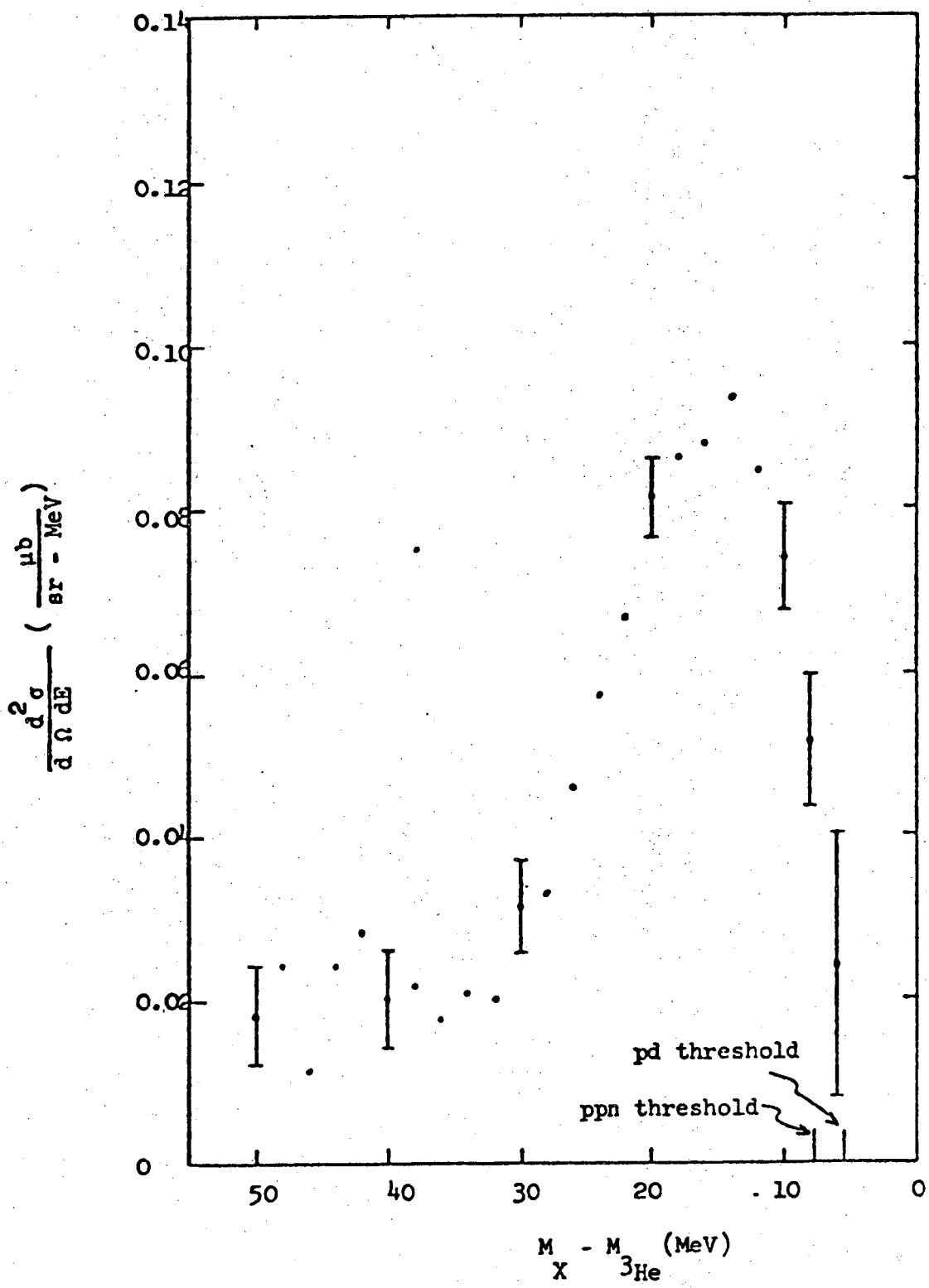

XBL 741-152

Fig. 15.

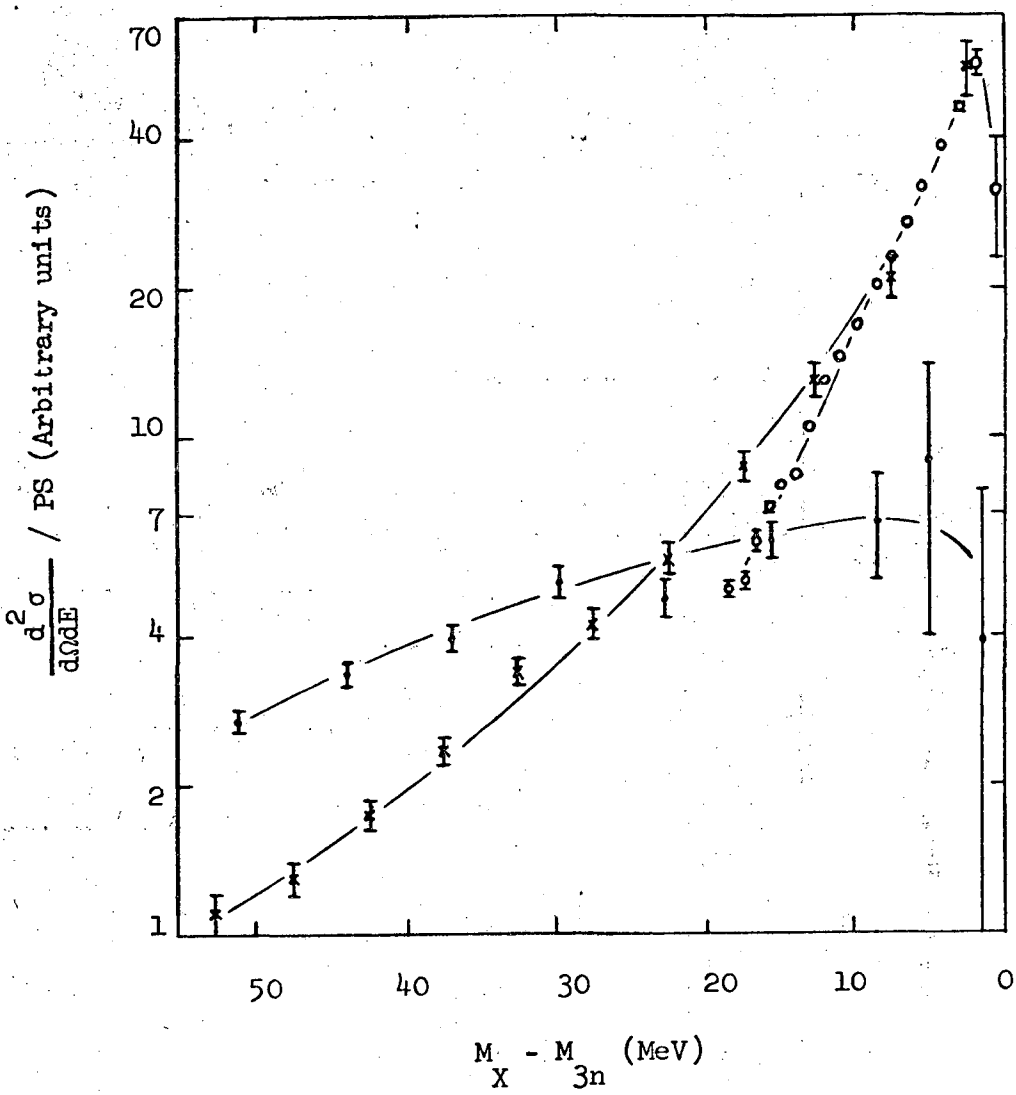

XBL 721-94

Fig. 16.

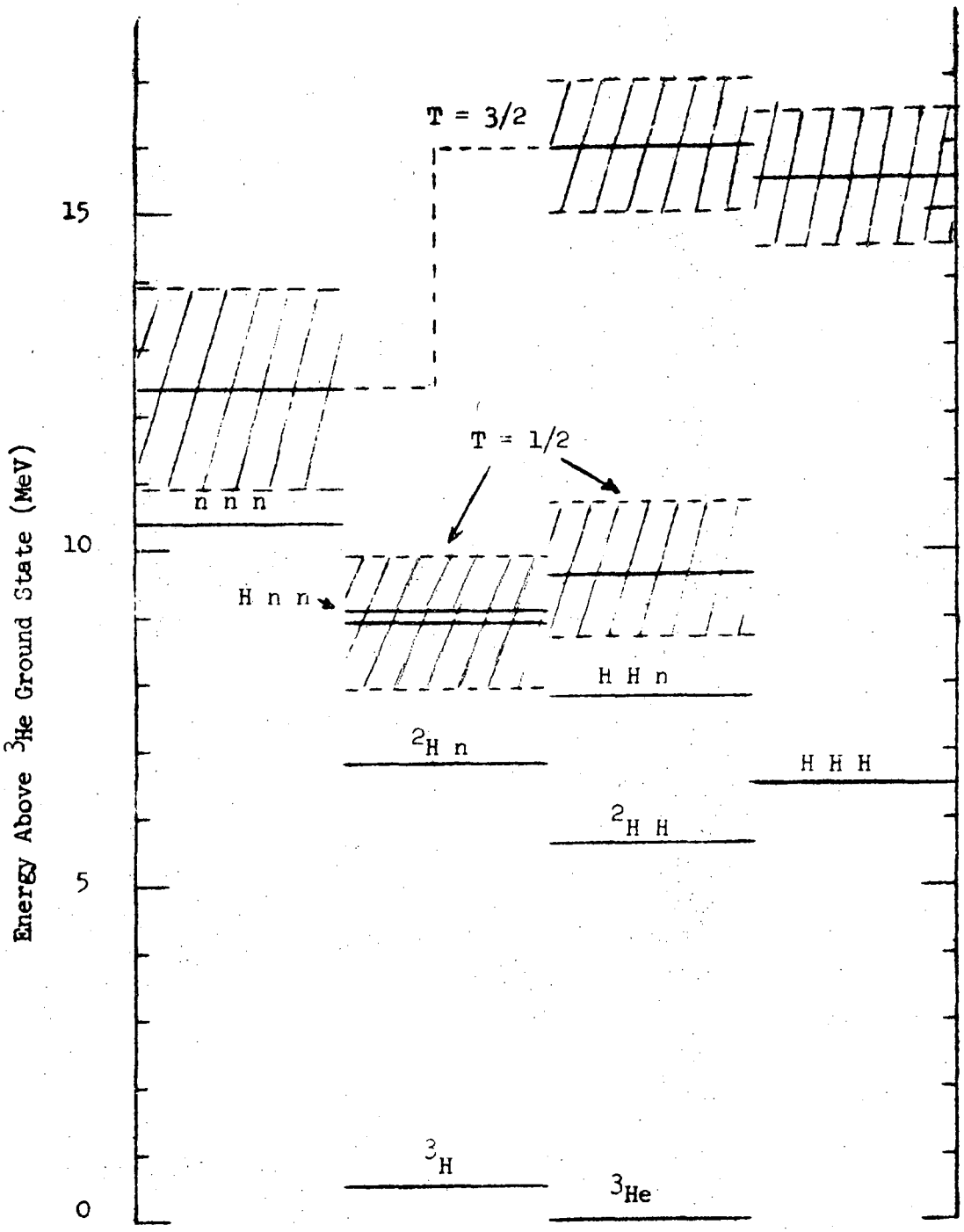

Energy Level Diagram for the A = 3 System

XBL 721-57

Fig. 17.

		3p excitation relative to the 3p threshold	$^3He^*$ excitation relative to the ground state	$^3H^*$ excitation relative to the ground state	3n excitation relative to the 3n threshold
$T = \frac{1}{2}$	This exp.		$E = 9.6 \pm 0.7$ MeV $\Gamma \approx 5$ MeV		
	Theory both pot. $S = \frac{3}{2}$ $L = 1$		$E \approx 9.0$ MeV	$E = 9.3$ MeV	
$T = \frac{3}{2}$	This exp.	$E = 9 \pm 1$ MeV $\Gamma \approx 10.5$ MeV	$E = 16 \pm 1$ MeV $\Gamma \approx 9$ MeV		1.0 to 1.5 MeV Ohlsen et al.
	AT-potential $S = \frac{1}{2}$ $L = 1$	$E = 5.5$ MeV	$E = 10.9$ MeV	$E = 10.6$ MeV $\Gamma = 1.6$ MeV	$E = 2.1$ MeV $\Gamma = 1.6$ MeV
	EH-potential $S = \frac{1}{2}$ $L = 1$	$E = 7.3$ MeV	$E = 12.6$ MeV	$E = 12.0$ MeV $\Gamma = 2.7$ MeV	$E = 3.5$ MeV $\Gamma = 2.6$ MeV

XBL 721-56

Fig. 18.

0 0 0 0 4 1 0 1 8 9 6

0 0 0 0 4 1 0 1 8 9 7

LEGAL NOTICE

This report was prepared as an account of work sponsored by the United States Government. Neither the United States nor the United States Atomic Energy Commission, nor any of their employees, nor any of their contractors, subcontractors, or their employees, makes any warranty, express or implied, or assumes any legal liability or responsibility for the accuracy, completeness or usefulness of any information, apparatus, product or process disclosed, or represents that its use would not infringe privately owned rights.

TECHNICAL INFORMATION DIVISION
LAWRENCE BERKELEY LABORATORY
UNIVERSITY OF CALIFORNIA
BERKELEY, CALIFORNIA 94720